DOI: 10.1002/ejic.200901108

Theoretical and Spectroscopic Investigation of Coordination Compounds from P_4S_3, Copper(I) Iodide and $W(CO)_5$

Gabor Balázs,[a] Andreas Biegerl,[a] Christian Gröger,[b] Joachim Wachter,*[a] Richard Weihrich,[a] and Manfred Zabel[a]

Keywords: Phosphorus / Sulfur / Copper / Tungsten / Coordination polymers / Density functional calculations

The formation of a new type of organometallic-inorganic hybrid coordination polymer from $P_4S_3{\cdot}W(CO)_5$ (**1**) and CuI has been studied. The structure of $\{P_4S_3{\cdot}W(CO)_5\}(CuI)$ (**3**) has been verified by the combination of spectroscopic (IR, Raman, ^{31}P MAS NMR) and X-ray diffraction methods. Theoretical studies of β-P_4S_3, $P_4S_3{\cdot}W(CO)_5$ (**1**), 1D-$(P_4S_3)(CuI)$ (**2**), and 3D-$(P_4S_3)(CuI)_3$ (**4**), which may be considered as potential building blocks of **3**, were carried out on the DFT level in the crystalline phase. The comparison of calculated and measured vibration modes of the P_4S_3 cage allows the unequivocal assignment of the recorded Raman shifts between 200 and 480 cm^{-1} and the determination of the degree of integration of P_4S_3 within the one-dimensional stacks of **2** or copper iodide networks of **3** and **4**.

Introduction

Tetraphosphorus sesquisulfide is a cage compound with fascinating coordination properties. The addition of $M(CO)_5$ fragments (M = Cr, Mo, W) to the apical phosphorus is, from a historical point of view, the most intensively studied reaction type since more than thirty years.[1] The simultaneous coordination of Lewis-acidic complex fragments or cations at basal and apical phosphorus has been reported only recently,[2] and even the participation of sulfur lone pairs could be realized.[3] The use of P_4S_3 as building block in copper(I) halide networks has stimulated a new kind of "soft" solid-state chemistry, for the formation of quaternary phases is achieved from solutions by interdiffusion techniques. Up to four cage phosphorus atoms are involved as coordination sites, but not sulfur.[4] The nature of the CuHal substructures depends on the employed halogen (Cl^- or I^-). The coordination behavior of CuBr is not as straightforward and will be reported elsewhere.[5]

Conventional solid-state techniques from the molten elements, phosphorus and sulfur, and CuI end up with the formation of $(P_4Q_4)(CuI)_3$ phases (Q = S, Se), in which β-P_4Q_4 cage molecules are embedded in polymeric matrices of copper iodide.[6,7] No hint has been obtained for the formation of P_4Q_3 containing phases, while CuCl or CuBr give rise to the formation of $PHal_3$. From crystallographic data of $(P_4Q_4)(CuI)_3$ it was concluded that there is only weak interaction between the phosphorus and the metal atoms.

The investigation of the nature of the interaction between cage molecules and Lewis acidic (LA) metal complex fragments requires theoretical analyses of the bonding properties of apical and basal coordination isomers of $P_4Q_3{\cdot}LA$ adducts, usually on the basis of gas phase model compounds.[2a,8] If structural data were available discrepancies between experimental and calculated data were observed.[9] Another efficient tool for the determination of bonding interactions is vibrational spectroscopy. Comparative Raman spectroscopy of an inorganic polymer is so far based on the empirical comparison of vibrational data of the polymer with those of the free molecule. Typical examples include $As_4S_4{\cdot}HgHal_2$ (Hal = Br, I), which exhibits very weak Hg–S interactions,[10] and $(As_4S_3)(CuCl)_n$ (n = 1,2), which is characterized by relatively strong As–S bonds.[11]

Recently, the influence of the condensed phase on DFT calculations has been described by Hocking, who examined metal–ligand bond lengths of coordination complexes by DFT methods in vacuo and condensed phase.[12] In this work we use the program package CRYSTAL06[13] to consider the influence of packing effects and intermolecular forces. It allows for a DFT approach on periodic structures successfully applied to calculate vibrational frequencies of pyrite type compounds.[14] Hybrid functionals like B3LYP can be used, too, to improve results for less dense structures like quartz or silicates significantly.[15] For comparison purposes and in order to get a deeper insight we studied Raman spectra of the series β-P_4S_3,[16] $P_4S_3{\cdot}W(CO)_5$ (**1**), one-dimensional $(P_4S_3)(CuI)$ (**2**),[4] and 3D-$(P_4S_3)(CuI)_3$ (**4**),[4] which are potential building blocks for the construction of $\{P_4S_3{\cdot}W(CO)_5\}(CuI)$ (**3**). All spectra except that of **3** are calculated by DFT methods in the crystalline phase. In or-

[a] Institut für Anorganische Chemie der Universität Regensburg, 93040 Regensburg, Germany
Fax: +49-941-943-4439
E-mail: Joachim.Wachter@chemie.uni-regensburg.de
[b] Institut für Biophysik und Physikalische Biochemie der Universität Regensburg, 93040 Regensburg, Germany

Supporting information for this article is available on the WWW under http://dx.doi.org/10.1002/ejic.200901108.

der to validate the new method the simulated vibrational frequencies of β-P_4S_3 and **1** are compared with data obtained from the gas phase and with measured Raman spectra.

Results

Syntheses and Structures

P_4S_3· W(CO)$_5$ (1): Reaction of a solution of P_4S_3 in THF with a slight excess of W(CO)$_5$THF gave yellow **1**. Its ^{31}P NMR spectrum exhibits two resonances which are in agreement with those described by Riess.[1e] The reaction of P_4S_3 with four to six equivalents of W(CO)$_5$THF gave an inseparable mixture of $P_4S_3\{W(CO)_5\}_n$ (n = 1, 2, 4) adducts, from which crystals of **1**, $P_4S_3\{W(CO)_5\}_2$ and $P_4S_3\{W(CO)_5\}_4$ were isolated and characterized by X-ray diffraction analyses. In all cases the W(CO)$_5$ fragments occupy the phosphorus sites of the cage.[17]

The molecular structure of **1** is analogous to that of P_4S_3·Mo(CO)$_5$.[1a] This means that a W(CO)$_5$ fragment is fixed at the apical P atom of the P_4S_3 cage (Figure 1). A comparison of bond features of the coordinated P_4S_3 molecule with those of the free cage reveals that all distances are less affected than in the case of P_4S_3·Mo(CO)$_5$. Compared to β-P_4S_3 the average distances within the cage are longer by 0.11 Å for $d(P_{apical}–S)$, equal for $d(P_{basal}–S)$ and longer by 0.022 Å for d(P–P).[16] A slight shortening of the bond W–C5 reflects the weak donor properties of the P_4S_3 ligand. The packing in the crystal is shown in Figure 2. Stacks of **1** are pairwise arranged so that the cage units lie in the crystallographic *ab* plain, whereas the W(CO)$_5$ units are linked together in a second plain parallel to the former. The closest intermolecular contacts within each layer are between 3.589 and 3.654 Å for d(P···S), what is close to the sum of van der Wals radii (3.75 Å) of phosphorus and sulfur.

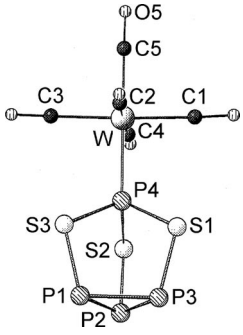

Figure 1. Molecular structure of **1**. Selected distances [Å]: W(1)–P(4) 2.448(2), W(1)–C(1) 2.055(10), W(1)–C(2) 2.026(12), W(1)–C(3) 2.060(11), W(1)–C(4) 2.058(12), W(1)–C(5) 2.031(10), S(1)–P(3) 2.094(3), S(1)–P(4) 2.098(4), S(2)–P(2) 2.089(3), S(2)–P(4) 2.096(3), S(3)–P(1) 2.095(3), S(3)–P(4) 2.098(4), P(1)–P(2) 2.246(4), P(1)–P(3) 2.242(4), P(2)–P(3) 2.247(4).

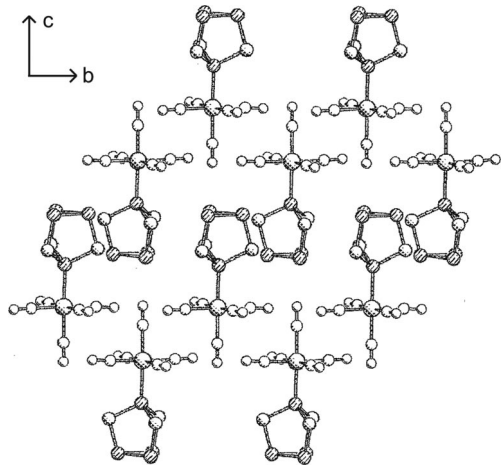

Figure 2. Section of the crystal structure of **1**; stacks viewed along *a*.

{P_4S_3· W(CO)$_5$}(CuI) (3): Layering a solution of CuI in CH_3CN over a solution of **1** in CH_2Cl_2 (molar ratio 1:1) gave after four days insoluble golden shining fibers of **3** in 84% yield. The composition of **3** follows from elemental analysis and has been confirmed by a preliminary X-ray crystallographic study. The IR spectrum reveals a ν(CO) absorption pattern at 2080, 2000 and 1940 cm^{-1}, which is typical of a W(CO)$_5$ fragment.

A crystal structure analysis of **3** has been attempted, but the quality of the structure solution has been handicapped by the extremely fine nature of the fibers. Inspite of this problem the heavy atom skeleton could be determined. The structure of **3** contains slightly twisted, castellated $(CuI)_n$ chains, which are linked by P_4S_3 cage molecules each contributing two basal P atoms (Figure 3). The resulting two-dimensional network is confined by W(CO)$_5$ fragments which are fixed at the apical phosphorus atoms of each of the P_4S_3 cages. Unfortunately, the CO groups could not be located but their presence is proved by the IR spectrum of **3**. Overall, the P_4S_3 cage serves for the first time as a tridentate ligand towards two different Lewis-acidic metal fragments. Further support of the proposed structure arises from solid-state ^{31}P MAS NMR and Raman spectra (see below).

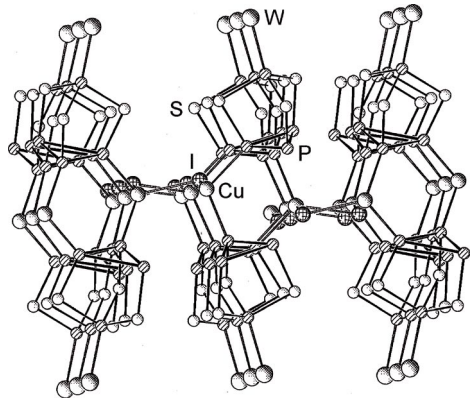

Figure 3. Section of the structure of **3** (CO groups omitted); stacks along *b*.

Raman Spectroscopy

Raman spectra of P_4S_3 (Figure 4) and compounds **1**–**4** have been measured. Spectra of **1** were calculated from the gas phase and, including those of P_4S_3, compared with data obtained from the condensed phase. An extension of the latter method on **2** and **4** and an extrapolation of the obtained data on **3** allows to determine the influence of copper or tungsten coordination on the P_4S_3 cage.

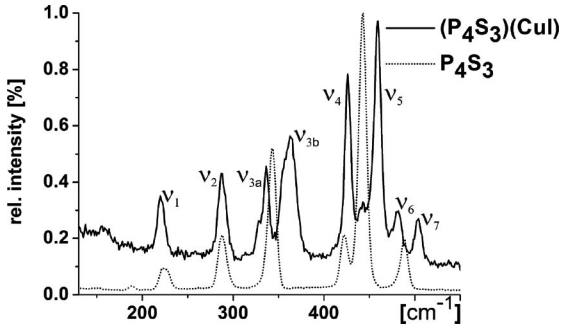

Figure 4. Experimental Raman spectra of P_4S_3 and **2**.

DFT Calculations

The normal mode frequencies and the corresponding vibrational assignments of P_4S_3 have already been calculated in the gas phase and compared with Raman frequencies of solid β-P_4S_3 (Table 1).[18–20] Jensen et al. calculated vibrational frequencies of P_4S_3 in more or less good agreement with experimental data by means of Hartree–Fock (HF) and second-order Moller-Plesset (MP2) methods. The best results were obtained with the density functional theory (DFT) method using the exchange correlation function B3LYP with the standard 6-31G* basis set, while HF and MP2 led to relatively big deviations (Table 1).[18] Then we carried out computational studies of frequencies of crystalline β-P_4S_3. The results, which are summarized in Table 1 and in Figure 5 show that there is still a better agreement with experimental Raman shifts.

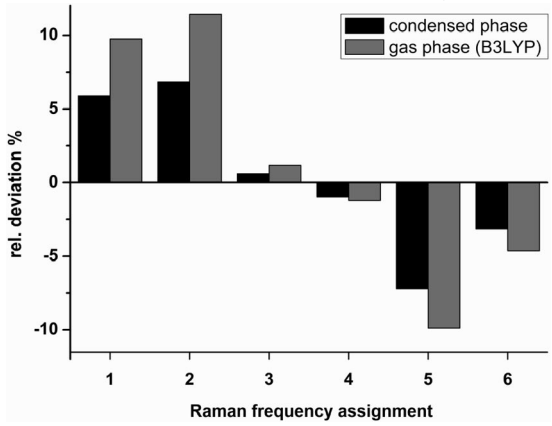

Figure 5. Relative deviations of DFT calculations of Raman frequencies of P_4S_3 in the gas phase[18] and in the condensed phase.

In the next step DFT calculations on $P_4S_3{\cdot}W(CO)_5$ (**1**) were performed in the gas phase with the Turbomole[21] program package using both, the BP86[22] and B3LYP[23] functionals with the TZVP basis set[24] for all atoms. Quasi-relativistic core potential was used for the tungsten atom. The calculated bond lengths are in agreement with the experimental ones, however they are slightly longer by 0.04 Å (mean). The vibrational frequencies calculated with the BP86 functional are in better agreement with the experimental data than those calculated with the B3LYP functional. Therefore, only the results obtained with the BP86 functional obtained without scaling are discussed.

The calculated vibrational spectra of **1** can be formally divided in a region up to 400 cm^{-1}, a second region from 400 to 600 cm^{-1} and a region around 2000 cm^{-1}. In the first and third region the vibrational frequencies are relatively well reproduced by calculations, however in the second region a strong coupling of the different vibration modes of the P_4S_3 skeleton with the CO groups of the $W(CO)_5$ unit was predicted but no direct experimental evidence for this coupling was found. This strong coupling prevents a clear assignment of different vibration modes by visualisation of the atomic displacements.

The comparison of calculated (216, 278 and 317 cm^{-1} assigned to P–S–P_{wag}, P–S–P_{bend} and P–$P_{stretch}$, respectively) and experimental Raman frequencies (223, 276 and 332 cm^{-1}) recorded for **1** (Figure 6, Table 2) allows for an unambiguous labelling. The frequencies ν_1, ν_2 and ν_3 calcu-

Table 1. Comparison of Raman shifts of P_4S_3, calculated in the gas phase and in the solid state (CRYSTAL06), with experimental shifts.

Jensen et al.[18]			Exp. Raman shifts	DFT/B3LYP[a]	Assignment
HF	MP2	DFT/B3LYP			
252	241	228	219	211	P–S–P wag, ν_1
332	307	296	283	270	P–S–P bend, ν_2
407	350	339	339	335	P–P stretch, ν_3
514	451	411	417	413	P–S–P stretch (a), ν_4
485	423	400	438	422	P–S–P stretch (s), ν_5
570	494	467	483	481	S–P stretch, ν_6

[a] Condensed phase, this work.

lated in the crystalline phase are of less accuracy, but the agreement is still good for these relatively large cells compared to SiO_2.[15] Furthermore, the comparison of the calculated vibrational modes of **1** with the experimental spectrum of P_4S_3 shows that the first three absorption bands are only slightly influenced by the coordination of the $W(CO)_5$ fragment. This observation is supported by the structural parameters (Figure 1). The experimental Raman shift at 367 cm^{-1} can be attributed to a P–S–P bending coupled with the ν(P–W) vibration. It is fairly reproduced by BP86 calculations (352 cm^{-1}), while it agrees well in the solid state (372 cm^{-1}). In the third region of the spectra, the calculated ν(CO) frequencies at 1974 and 1977 cm^{-1} are moderately shifted to higher wave numbers, whereas the calculated absorption at 2073 cm^{-1} is only slightly shifted to lower wave numbers compared to the experimental data [ν(CO) = 1927, 1945, 2081 cm^{-1}]. The increasing number of ν(CO) absorptions may be explained by a decrease of C_{4v} symmetry (local symmetry) of the $W(CO)_5$ fragment to C_{2v} (or C_s) in the gas phase model and packing effects in the crystal.

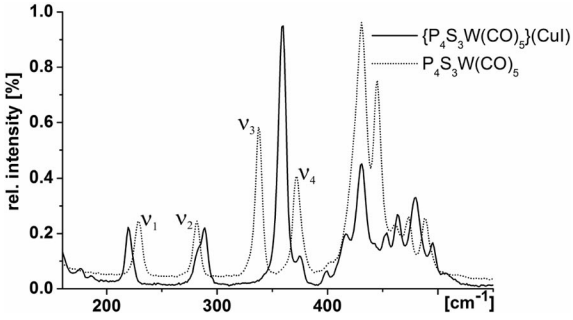

Figure 6. Experimental Raman spectra of **1** and $\{P_4S_3 \cdot W(CO)_5\}$-(CuI).

Table 2. Experimental and calculated IR wavenumbers and Raman shifts of **1**.

	IR wavenumbers (cm^{-1})			
ν̃(CO) (KBr)	CRYSTAL06		Turbomole	
2081 s	2094		2073	
	2015		–	
	1955		1977	
1945 vs	1952		1974	
1927 sh	1931		–	
	Raman shifts (cm^{-1})			
Freq. no.	CRYSTAL06	Turbomole	exp.	Assignment
ν_1	210	216	223	$P–S–P_{wag}$
ν_2	267	278	276	$P–S–P_{bend}$
ν_3	311	317	332	$P–P_{stretch}$
ν_4	372	352	367	$P–S–P_{bend}$/P–W

In a further step we performed calculations on copper iodide coordination compounds with P_4S_3. As a first example we took $(P_4S_3)(CuI)$ (**2**), which is a one-dimensional polymer composed of Cu_2I_2 four-membered rings bridged by P_4S_3 units (Figure 7).[4] As an extension of this work we got qualitative information on the shielding trends in ^{31}P MAS NMR spectroscopy in **2**.

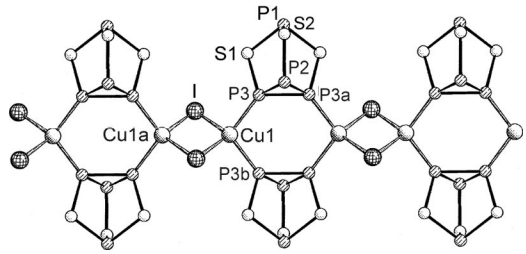

Figure 7. Section of the structure of **2**.[4]

The calculated Raman shifts of **2** agree well with the experimental data and there is no need to introduce scaling factors (Table 3). The vibrational modes are assigned by calculation. A comparison of the measured Raman spectra of P_4S_3 and **2** (Figure 4) reveals the existence of two groups of frequencies. Whereas ν_1 and ν_2 are only marginally shifted, what can be ascribed to the fact that the basis of the coordinated P_4S_3 cage is not involved in these modes, the other frequencies are affected by the coordination to copper sites. The P–P stretching of P_4S_3 at 339 cm^{-1} (ν_3) is influenced by coordination and the frequency splits into two ones because of symmetry mutations of the coordinated P_3 basis compared to the free P_4S_3 basis. The symmetric P–P stretching can be observed at 331 cm^{-1} (ν_{3a}), whereas the antisymmetric P–P stretching can be identified at 354 cm^{-1} (ν_{3b}). As a result, the uncoordinated phosphorus atom is able to vibrate easier than the coordinated basal phosphorus atoms. This is also reflected by a small increase of these bonds in the crystal structure of $(P_4S_3)(CuI)$ by 0.044(1) Å.

Table 3. Experimental and calculated Raman shifts (cm^{-1}) of **2** and **4** in comparison to P_4S_3.

Freq. no.	**2**		**4**		P_4S_3 (exp.)
	calcd.	exp.	calcd.	exp.	
ν_1	209	215	215	215	219
ν_2	278	282	259	274	283
ν_{3a}	328	331	310	294	339
ν_{3b}	346	354	344	352[a]	–
ν_4	419	421	433	438	417
ν_5	450	454	448	462	438
ν_6	476	477	493	498	483
ν_7	496	499			–

[a] Vibrations at 355 and 370 cm^{-1} cannot clearly be resolved (see text).

Important differences are also observed for the modes in which the sulfur bridges are involved. Thus, for P_4S_3 a symmetric P–S–P stretching (ν_4) is observed at 417 cm^{-1} whereas antisymmetric P–S–P stretching (ν_5) is found at 438 cm^{-1}. In **2** these Raman shifts are split into two vibrations which arise from participation of both coordinated phosphorus atoms of the basis, while the free basal phosphorus atom is hardly incorporated into the stretching modes. As a result the symmetric P–S–P stretching mode appears at 421 cm^{-1} (ν_4) and the antisymmetric P–S–P stretching mode at 454 cm^{-1} (ν_5). The stretching of $S–P_{apical}$ is only slightly affected (ν_6) by the incorporation of the cage in the polymeric chain when compared to P_4S_3.

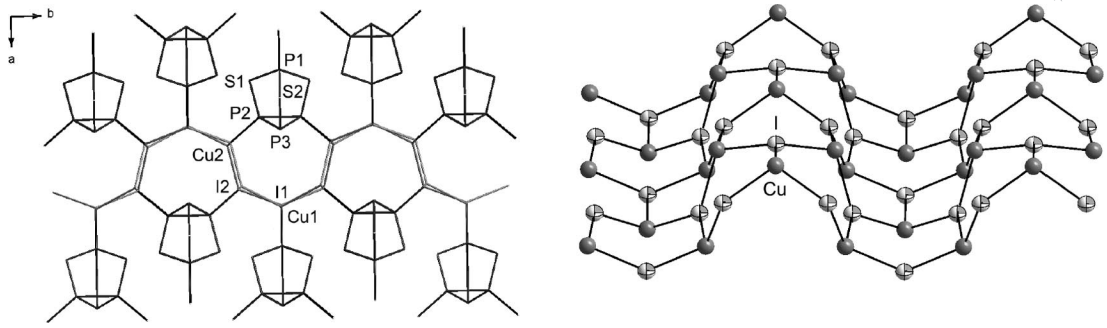

Figure 8. Section of the structure (left) and the $(CuI)_n$ network (right) of **4**.[4]

The Raman spectrum of **3** shows a relatively simple pattern between 200 and 400 cm^{-1} (Figure 6). The most striking difference in this region is the shift of ν_3 ($P–P_{stretch}$) from 332 cm^{-1} in **1** to 360 cm^{-1}, which is accompanied by an increase in intensity. The weak vibration at 375 cm^{-1} is tentatively assigned to ν(P–W), similar to that of **1**. The region between 400 and 500 cm^{-1} shows similarities to the spectrum of **1** thus reflecting a similar coupling of the different vibration modes of the P_4S_3 cage with the CO groups of the $W(CO)_5$ unit. For these reasons a closer theoretical examination of the spectrum of **3** was not attempted.

In the following an extension of the calculations from one- to three-dimensional polymers is demonstrated. As a representative example we took 3D-$(P_4S_3)(CuI)_3$, the structure of which consists of undulated $(CuI)_n$ layers which are linked by tridentate P_4S_3 ligands (Figure 8).[4] Two atoms of the P_3 basis form columns upon linking two fused six-membered Cu_3I_3 ring-subunits of one and the same $(Cu_3I_3)_n$ layer, while the apical phosphorus atom coordinates to Cu of the next sheet thus forming seven-membered columns. The Raman spectrum of $(P_4S_3)(CuI)_3$ is shown in Figure 9, the comparison of calculated and experimental data is given in Table 3. It is striking that the frequencies ν_1–ν_6 correspond to those found for **2**. The frequency at 185 cm^{-1} may be clearly assigned to a $\nu(P_{ap}–Cu)$ vibration, not present in the spectra of **1**–**3**. The additional frequencies at 355 and 370 cm^{-1} are difficult to assign, because the calculated shifts for vibrations of symmetries B_{1g} and B_{2g}, which are found in the respective region, are very close to each other.

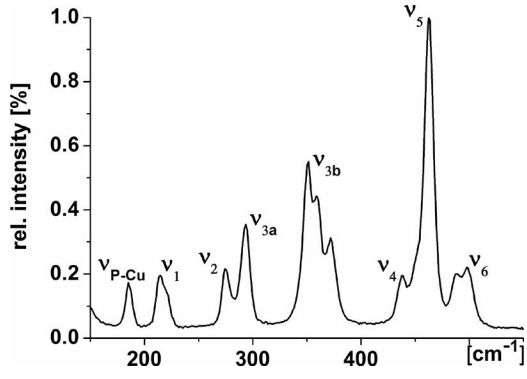

Figure 9. Raman spectrum of **4**.

^{31}P MAS NMR Spectroscopy

More structural information on the new compounds **1** and **3** may be obtained by solid-state ^{31}P MAS NMR spectroscopy. The coordination of $W(CO)_5$ at the apical P atom of the cage gives rise to a slight downfield shift of 3.7 (**1**) or 10.1 ppm (**3**) compared to P_4S_3 (Table 4). The spectrum of **3** exhibits a further group of signals (Figure 10), which after simulation split into a singlet at –77.8 ppm and two multiplets at –84.1 ppm ($J_{Cu,P}$ = 854 Hz) and –93.5 ppm ($J_{Cu,P}$ = 717 Hz), respectively. The observed pattern indicates a slight inequivalency of the two P atoms bearing copper, probably caused by a slight anisotropy within the crystal structure (Figure 3). Unfortunately, the actual state of the structure solution does not provide more precise information.

Table 4. ^{31}P MAS NMR chemical shifts (δ in ppm) and coupling constants $^{31}P–^{63/65}Cu$ (J in Hz) of β-P_4S_3 and compounds **1**–**4**.

	P_{apical}	P_{basal}
β-P_4S_3[31]	81.8 s	–102.7 s
P_4S_3·$W(CO)_5$ (**1**)	85.5 s	–110.7 s
$(P_4S_3)(CuI)$ (**2**)[4]	113.8 s	–82.8 m (900), –95.3 s
{P_4S_3·$W(CO)_5$}(CuI) (**3**)	92.9 s	–77.8 s, –84.1 m (854), –93.5 m (717)
$(P_4S_3)(CuI)_3$[4] (**4**)[4]	82.2 m (1100)	–94.2 m (698), –94.9 s

A comparison of ^{31}P MAS NMR spectra of **1**, **2** and **3** shows that the chemical shift of the apical phosphorus atom of the P_4S_3 cage in **3** is slightly shifted to low field by $W(CO)_5$ coordination (Table 4). Interestingly, the lowest chemical shift is found in the 1D-polymer **2** (see below). The resonances of the basal phosphorus atoms of **2**–**4** are shifted to low field between $\Delta(\delta)$ = 24.9 (**3**) and 7.8 ppm (**4**) with respect to P_4S_3. The observed trends are contradictory to those observed for $P_4Se_4(CuI)_3$[25] or $P_4S_4(CuI)_3$[26] in which the cage molecules are embedded in copper iodide networks. For both examples significant shielding effects have been proposed as a consequence of the coordination of Cu^I to P sites.

Although the apical P atom of **2** does not coordinate to copper the corresponding resonance is remarkably shifted to low field with respect to β-P_4S_3 (Table 4). A similar shift of the same order [$\Delta(\delta)$ = 32 ppm] has been found in 1D-$(P_4S_3)(CuBr)$.[5] In order to understand this anomaly of chemical shifts we have carried out a Mulliken population analysis of the total electron distribution in the solid state

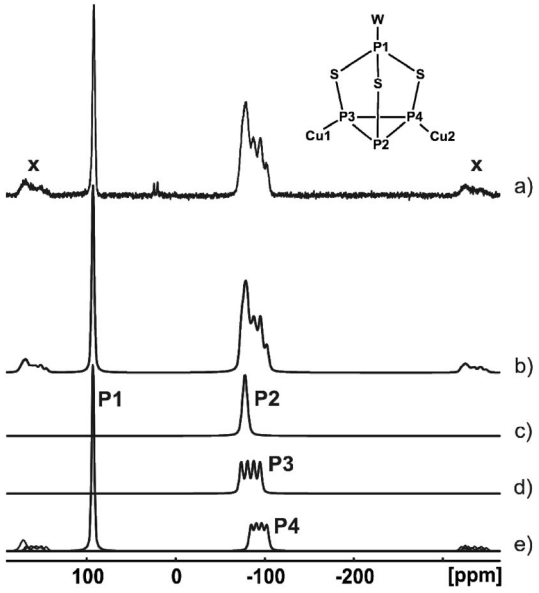

Figure 10. Solid-state ^{31}P MAS NMR spectra of **3**. a) Experimental spectrum; b) simulated spectrum; c–e) simulated spectra showing individual components. Spinning side bands are marked by the symbol ×; the assignment of P3 and P4 is arbitrary.

with the CRYSTAL 06 program package for P_4S_3, **2**, and **4**. The same basis sets were employed as for the calculation of the vibrational spectra. Qualitatively it could be shown that the 3s orbital electron distribution of the apical P atoms is nearly the same for P_4S_3 and $(P_4S_3)(CuI)_3$, but decreases significantly for **2**. This result corresponds perfectly to the trend observed for the ^{31}P chemical shifts of the concerned compounds. The origin of this effect is still unclear, for there are no striking deformations within the P_4S_3 cage nor are there significant contacts between stacks of 1D-$(P_4S_3)(CuI)$ chains in the crystal.[4]

Conclusions

The new organometallic-inorganic hybrid coordination polymer $\{P_4S_3{\cdot}W(CO)_5\}(CuI)$ (**3**) has been formed from $P_4S_3{\cdot}W(CO)_5$ (**1**) and CuI. The structure of **3** has been solved by the combination of spectroscopic (IR, Raman, ^{31}P MAS NMR) and X-ray diffraction methods. Theoretical studies of the potential building blocks β-P_4S_3, **1**, 1D-$(P_4S_3)(CuI)$ (**2**) and 3D-$(P_4S_3)(CuI)_3$ (**4**) have been carried out on the DFT level in the crystalline phase. The new method is able to consider the influence of the solid state such as packing effects and intermolecular forces and it replaces calculations of molecular model compounds, which are often sections of polymers in the gas phase. The obtained results lead to a better agreement of computed Raman frequencies with experimental data.

Experimental Section

General: All manipulations were carried out under nitrogen by Schlenk techniques. Usually, the diffusion experiments were carried out in Schlenk tubes of 3.0 cm diameter, if not otherwise stated. P_4S_3 was synthesized by melting red phosphorus and sulfur in a molar ratio of 5 to 3 under a nitrogen atmosphere. P_4S_3 was extracted by toluene and purified by recrystallisation from CH_2Cl_2. ^{31}P MAS NMR spectra were recorded on a Bruker Advance 300 spectrometer using a double resonance 2.5 mm MAS probe. The ^{31}P resonance was 121.495 MHz. All spectra were acquired at a MAS rotation frequency of 35 kHz, a 90° pulse length of 2.3 μs and with a relaxation delay of 450 s. For spectrum simulation the program DMFIT was used.[27] The Raman spectra were taken by reflection with an Andor DV401 CCD detector. The excitation of the microcrystalline samples were carried out with a HeNe laser (λ = 632.8 nm).

CRYSTAL06 Computational Details: The calculations were performed within the framework of DFT theory as implemented in the LCAO-code CRYSTAL06.[13,28] Therein, the electronic structure is calculated from Gaussian type local basis sets. IR and Raman frequencies are calculated from the vibrational spectra at the gammma point.[29] Exchange and correlation were treated as described by the B3LYP functional for all results presented in this paper. All electron basis sets were used for Cu (0.28, 0.4), and O (0.24, 0.5), valence basis sets for P (0.23, 0.49), S (0.22, 0.44), I (0.22, 0.33), and W (0.25, 0.26) with respective optimized coefficients for outer (sp, d) functions.[30] The calculations were convergenced to total energy $\Delta E < 10^{-8}$ H applying a *k*-points shrinking factors of 4 to 8 and Anderson mixing (see ref.[13]).

Syntheses

$P_4S_3{\cdot}W(CO)_5$: P_4S_3 (300 mg, 1.36 mmol) was added to a $W(CO)_5$ THF solution (2.045 mmol, c = 28 mmol L^{-1}). The reaction mixture was stirred at room temperature and the solvent was removed after 20 h. The reaction product was washed three times with small amounts of toluene and yellow powder of **1** (yield 555 mg, 78%) was obtained. ^{31}P{^{1}H} NMR (300 MHz, C_6D_6): δ = 85.5 (q, $J_{P,P}$ = 31, $J_{P,W}$ = 126 Hz), –110.4 (d, $J_{P,P}$ = 31 Hz) ppm. $C_5O_5P_4S_3W$ (543.98): calcd. C 11.04, S 17.68; found C 11.02, S 17.81. IR [KBr, $\tilde{\nu}$(CO)]: $\tilde{\nu}$ = 2083 (s), 2000 (w), 1938 (br) cm^{-1}.

$\{P_4S_3{\cdot}W(CO)_5\}(CuI)$: A solution of CuI (18 mg, 0.092 mmol) in CH_3CN (10 mL, c = 9 mmol L^{-1}) was layered carefully over a solution of **1** (50 mg, 0.092 mmol) in 20 mL CH_2Cl_2 (c = 5 mmol· L^{-1}). After four days golden shining fibers of **3** crystallized. The product was washed with a CH_2Cl_2/CH_3CN mixture and dried under vacuum. Yield 51 mg (75%); ^{31}P MAS NMR (300 MHz): δ = 92.9 (s), –77.8 (s), –84.1 [m, J(Cu,P) = 854 Hz], –93.5 [m, J(Cu,P) = 717 Hz] ppm. $C_5CuIO_5P_4S_3W$ (734.47): calcd. C 8.18, S 13.10; found C 7.97, S 12.73. IR [KBr, $\tilde{\nu}$(CO)]: $\tilde{\nu}$ = 2080 (vs), 2000 (s), 1940 (br) cm^{-1}.

Crystal Structure Analyses: 1: Data were collected on an Oxford Diffraction Gemini Ultra diffractometer (Cu-K_α radiation) at 123 K. The structure was solved by direct methods and refined by full-matrix least-squares (SHELXL97 program) with all reflections. Yellow needles, 0.17 × 0.09 × 0.08 mm^3, triclinic, $P\bar{1}$, a = 6.950(3), b = 8.998(4), c = 11.559(6) Å, α = 87.2(0), β = 82.8(0), γ = 81.13(0)°. V = 708.26(6) Å^3, Z = 2, $\rho_{calcd.}$ = 2.551 g/cm^{-3}, θ = 4.98–62.20°, μ = 23.635 mm^{-1}, 6629 measured reflections, 2191 independent reflections (R_{int} = 0.0304), 2039 observed reflections [$I > 2\sigma(I)$], 163 refined parameters, $R1$ (all data) = 0.0420, $wR2$ = 0.1091, residual electron density 2.688/–1.231 e·Å^{-3}.

CCDC-757374 (for **1**) contains the crystallographic data (excluding structure factors). These data can be obtained free of charge from The Cambridge Crystallographic Data Centre via www.ccdc.cam.ac.uk/data_request/cif.

Supporting Information (see also the footnote on the first page of this article): Atomic displacements of the key vibrational modes of P_4S_3, **1**, **2** and **4**.

Acknowledgments

This work was supported by the Deutsche Forschungsgemeinschaft (DFG) (Wa 486/11-1 and We 4284/1-1). We gratefully acknowledge continuous support by Prof. Dr. M. Scheer. R. W. thanks Prof. R. Dovesi for fruitful discussions. We also thank Dipl. Chem. C. Güntner for technical assistance in recording the Raman spectra.

[1] a) A. W. Cordes, R. D. Joyner, R. D. Shores, E. D. Dill, *Inorg. Chem.* **1974**, *13*, 132; b) R. Jefferson, H. F. Klein, J. F. Nixon, *J. Chem. Soc. C* **1969**, 536; c) M. Di Vaira, M. Peruzzini, P. Stoppioni, *J. Organomet. Chem.* **1983**, *258*, 373; d) M. Di Vaira, M. Peruzzini, P. Stoppioni, *Inorg. Chem.* **1983**, *22*, 2196; e) J. G. Riess, *ACS Symp., Ser.* **1983**, *232*, 17.

[2] a) E. Guidoboni, I. de los Rios, A. Ienco, L. Marvelli, C. Mealli, A. Romerosa, R. Rossi, M. Peruzzini, *Inorg. Chem.* **2002**, *41*, 659; b) M. Di Vaira, I. de los Rios, F. Mani, M. Peruzzini, P. Stoppioni, *Eur. J. Inorg. Chem.* **2004**, 293; c) I. de los Rios, F. Mani, M. Peruzzini, P. Stoppioni, *Inorg. Chem.* **2004**, *43*, 164; d) P. Barbaro, M. Di Vaira, M. Peruzzini, S. S. Constantini, P. Stoppioni, *Chem. Eur. J.* **2007**, *13*, 6682.

[3] a) A. Adolf, M. Gonsior, I. Krossing, *J. Am. Chem. Soc.* **2002**, *124*, 7111; b) I. Raabe, S. Antonijevic, I. Krossing, *Chem. Eur. J.* **2007**, *13*, 7510.

[4] A. Biegerl, E. Brunner, C. Gröger, M. Scheer, J. Wachter, M. Zabel, *Chem. Eur. J.* **2007**, *13*, 9270.

[5] A. Biegerl, C. Gröger, H. R. Kalbitzer, J. Wachter, M. Zabel, *Z. Anorg. Allg. Chem.*, in press.

[6] S. Reiser, G. Brunklaus, J. H. Hong, J. C. C. Chan, H. Eckert, A. Pfitzner, *Chem. Eur. J.* **2002**, *8*, 4228.

[7] a) A. Pfitzner, S. Reiser, H.-J. Deiseroth, *Z. Anorg. Allg. Chem.* **1999**, *625*, 2196; b) A. Pfitzner, S. Reiser, *Inorg. Chem.* **1999**, *38*, 2451.

[8] J. D. Head, K. A. R. Mitchell, L. Noodleman, N. L. Paddock, *Can. J. Chem.* **1977**, *55*, 669.

[9] C. Aubauer, E. Irran, T. M. Klapötke, W. Schnick, A. Schulz, J. Senker, *Inorg. Chem.* **2001**, *40*, 4956.

[10] a) M. F. Bräu, A. Pfitzner, *Angew. Chem.* **2003**, *118*, 4576–4578; *Angew. Chem. Int. Ed.* **2006**, *45*, 4464; b) M. F. Bräu, A. Pfitzner, *Z. Anorg. Allg. Chem.* **2007**, *633*, 935.

[11] P. Schwarz, J. Wachter, M. Zabel, *Eur. J. Inorg. Chem.* **2008**, 5460.

[12] R. K. Hocking, R. J. Deeth, T. W. Hambley, *Inorg. Chem.* **2007**, *46*, 8238.

[13] R. Dovesi, V. R. Saunders, C. Roetti, R. Orlando, C. M. Zicovich-Wilson, F. Pascale, B. Civalleri, K. Doll, N. M. Harrison, I. J. Bush, P. D'Arco, M. Llunell, CRYSTAL06, user's guide, Torino, **2006**.

[14] M. Meier, R. Weihrich, *Chem. Phys. Lett.* **2008**, *461*, 38.

[15] C. M. Zicovich-Wilson, F. Pascale, C. Roetti, V. R. Saunders, R. Orlando, R. Dovesi, *J. Comput. Chem.* **2004**, *25*, 1873.

[16] a) T. K. Chattopadhyay, M. May, H. G. von Schnering, G. S. Pawley, *Z. Kristallogr.* **1983**, *165*, 47; b) U. Müller, H. Gruber, *Z. Kristallogr.* **1997**, *212*, 662.

[17] A. Biegerl, J. Wachter, unpublished results.

[18] J. O. Jensen, D. Zeroka, A. Banerjee, *THEOCHEM* **2000**, *505*, 31.

[19] M. Gardner, *J. Chem. Soc., Dalton Trans.* **1973**, 691.

[20] M. Ystenes, W. Brockner, F. Menzel, *Vib. Spectrosc.* **1993**, *5*, 195.

[21] a) R. Ahlrichs, M. Bär, M. Häser, H. Horn, C. Kölmel, *Chem. Phys. Lett.* **1989**, *162*, 165; b) O. Treutler, R. Ahlrichs, *J. Chem. Phys.* **1995**, *102*, 346; c) http://www.turbomole-gmbh.com/.

[22] a) A. D. Becke, *Phys. Rev. A* **1988**, *38*, 3098; b) S. H. Vosko, L. Wilk, M. Nusair, *Can. J. Phys.* **1980**, *58*, 1200; c) J. P. Perdew, *Phys. Rev. B* **1986**, *33*, 8822; Erratum: J. P. Perdew, *Phys. Rev. B* **1986**, *34*, 7406.

[23] a) P. A. M. Dirac, *Proc. R. Soc. London, Ser. A* **1929**, *123*, 714; b) J. C. Slater, *Phys. Rev.* **1951**, *81*, 385; c) S. H. Vosko, L. Wilk, M. Nusair, *Can. J. Phys.* **1980**, *58*, 1200; d) A. D. Becke, *Phys. Rev. A* **1988**, *38*, 3098; e) C. Lee, W. Yang, R. G. Parr, *Phys. Rev. B* **1988**, *37*, 785; f) A. D. Becke, *J. Chem. Phys.* **1993**, *98*, 5648.

[24] a) A. Schäfer, C. Huber, R. Ahlrich, *J. Chem. Phys.* **1994**, *100*, 5829; b) K. Eichkorn, F. Weigend, O. Treutler, R. Ahlrichs, *Theor. Chem. Acc.* **1997**, *97*, 119.

[25] G. Brunklaus, J. C. C. Chan, H. Eckert, S. Reiser, T. Nilges, A. Pfitzner, *Phys. Chem. Chem. Phys.* **2003**, *5*, 3768.

[26] S. Reiser, G. Brunklaus, J. H. Hong, J. C. C. Chan, H. Eckert, A. Pfitzner, *Chem. Eur. J.* **2002**, *8*, 4228.

[27] D. Massiot, F. Fayon, M. Capron, I. King, S. Le Calvé, B. Alonso, J.-O. Durand, B. Bujoli, Z. Gan, G. Hoatson, *Magn. Reson. Chem.* **2002**, *40*, 70.

[28] M. D. Towler, M. Causa, A. Zupan, *Comput. Phys. Commun.* **1996**, *98*, 181.

[29] F. Pascale, C. M. Zicovich-Wilson, F. Lopez Gejo, B. Civalleri, R. Orlando, R. Dovesi, *J. Comput. Chem.* **2004**, *25*, 888.

[30] Crystal basis set library: http://www.crystal.unito.it/Basis_Sets/Ptable.html.

[31] a) R. K. Harris, P. J. Wilkes, P. T. Wood, J. D. Woollins, *J. Chem. Soc., Dalton Trans.* **1989**, 809; b) H. Eckert, C. S. Liang, G. D. Stucky, *J. Phys. Chem.* **1989**, *93*, 452; c) I. Raabe, S. Antonijevic, I. Krossing, *Chem. Eur. J.* **2007**, *13*, 7510.

Received: November 17, 2009
Published Online: February 4, 2010

